Mononuclear Lanthanide SMMs

International Edition: DOI: 10.1002/anie.201411190
German Edition: DOI: 10.1002/ange.201411190

A Trigonal-Pyramidal Erbium(III) Single-Molecule Magnet**

*Andrew J. Brown, Dawid Pinkowicz, Mohamed R. Saber, and Kim R. Dunbar**

Abstract: *Given the recent advent of mononuclear single-molecule magnets (SMMs), a rational approach based on lanthanides with axially elongated f-electron charge cloud (prolate) has only recently received attention. We report herein a new SMM, $[Li(THF)_4[Er\{N(SiMe_3)_2\}_3Cl]\cdot 2\,THF$, which exhibits slow relaxation of the magnetization under zero dc field with an effective barrier to the reversal of magnetization ($\Delta E_{eff}/k_B = 63.3$ K) and magnetic hysteresis up to 3 K at a magnetic field sweep rate of 34.6 Oe s^{-1}. This work questions the theory that oblate or prolate lanthanides must be stabilized with the appropriate ligand framework in order for SMM behavior to be favored.*

Lanthanide-containing mononuclear single-molecule magnets (SMMs) have received much attention in the last five years,[1] as they appear to be the best candidates in the field of molecular magnetism for application in high density data storage, molecular spintronics, and quantum processing.[2] The advantages of 4f elements stem from their inherent anisotropy imparted by high ground state spin values and strong spin–orbit coupling, producing an oblate or prolate shape for the 4f electron density, which can be stabilized by a ligand field of the appropriate symmetry.[3]

By using geometric design principles to minimize electronic repulsions between the electron densities of the lanthanide ions and the ligands, researchers have prepared SMMs with extremely high barriers and magnetic hysteresis as compared to previous examples.[4] While most examples of the rare-earth SMMs are based on the oblate terbium and dysprosium ions (and particularly the latter[5]) more recent work has revealed that prolate ions can also engender SMM behavior, with the erbium(III) ion being the main choice for such systems.[6] The first reported erbium(III) mononuclear SMM is the organometallic complex [(Cp*)Er(COT)] (Cp* = pentamethylcyclopentadienide; COT = cyclooctatetraenide), reported by Gao and co-workers, which exhibits two relaxation processes with energy barriers $\Delta E_{eff}/k_B$ of 197 and 323 K and a butterfly hysteresis loop as high as 5 K.[6a] More recently, Long and co-workers prepared $[Er(COT)_2]^-$, which exhibits enhanced SMM properties because the equatorial nature of the ligands is more compatible with preserving the prolate nature of the erbium(III) ion electron density and the molecule is symmetrical. The compound exhibits a high energy barrier of $\Delta E_{eff}/k_B = 216$ K with waist-restricted hysteresis being observed at temperatures up to 10 K for a diluted sample in a yttrium matrix.[6b] Murugesu and co-workers also studied this system[7] and derivatized the COT ligand with trimethylsilyl appendages to study the effects of lowering the symmetry. Both $[Er(COT'')_2]^-$ and $[Er_2(COT'')_3]$ (COT'' = 1,4-bis(trimethylsilyl)cyclooctatetraenyl dianion) were prepared,[6c] and it was found that the double-decker sandwich compound exhibits $\Delta E_{eff}/k_B = 335$ K and hysteresis up to 14 K in solution.[8]

Along with the rare-earth organometallic sandwich compounds, there are also low-coordinate species of the type $[Ln\{N(SiMe_3)_2\}_3]$ that have been studied for catalysis.[9] The bis(trimethylsilyl)amide ligand is known to enforce a trigonal planar geometry in transition metal complexes,[10] but the lanthanide analogues are distorted towards a trigonal pyramidal structure due to agostic interactions between the lanthanide center with the β-Si–C bond of the ligand, as well as bonding considerations involving the d-orbitals of the lanthanide ion.[11] Tang and co-workers recently reported the magnetic properties of $[Er\{N(SiMe_3)_2\}_3]$, the first example of an equatorially coordinated mononuclear lanthanide SMM; the molecule exhibits a blocking temperature of about 13 K based on the χ''(T) maximum at a frequency of 1488 Hz and a barrier to the reversal of magnetization $\Delta E_{eff}/k_B = 122$ K with hysteresis reported to occur at 1.9 K.[12] They also reported $[Er(NHPh\textit{i}Pr_2)_3(THF)_2]$, which exhibits SMM behavior only in the presence of a dc field.

Recently we also prepared $[Er\{N(SiMe_3)_2\}_3]$ for the aforementioned reasons, but during the course of this work, the results of Tang and co-workers appeared. We therefore decided to pursue the properties of a related compound with a bridging chloride that we isolated from one of the syntheses under specific conditions (see note in synthesis section of Supporting Information for **1**). Herein we report the preparation, crystal structure, and magnetic characterization of $[Li(THF)_4][Er\{N(SiMe_3)_2\}_3Cl]\cdot 2\,THF$ (**1**). The effects of solid-state dilution with the yttrium complex are also reported. While analogues with other lanthanide ions exist,[13] the erbium(III) congener was not reported previously. Interestingly, compound **1** exhibits improved magnetic properties as compared with $[Er(NHPh\textit{i}Pr_2)_3(THF)_2]$ despite the presence of a rigorously axial and negatively charged chloride. These

[*] A. J. Brown, Dr. M. R. Saber,[+] Prof. K. R. Dunbar
Department of Chemistry, Texas A&M University
College Station, TX 77843 (USA)
E-mail: dunbar@chem.tamu.edu
Homepage: http://www.chem.tamu.edu/rgroup/dunbar/
Dr. D. Pinkowicz
Faculty of Chemistry, Jagiellonian University
Ingardena 3, 30-060 Kraków (Poland)
[+] Permanent address: Department of Chemistry
Fayoum University, Fayoum 63514 (Egypt)

[**] This material is based on work supported by the US Department of Energy, Materials Sciences Division, under Grant No. DE-SC0012582. D.P. gratefully acknowledges the financial support of the EC REA within the Marie Curie International Outgoing Fellowship, project MultiCyChem (grant agreement no. PIOF-GA-2011-298569).

Supporting information for this article is available on the WWW under http://dx.doi.org/10.1002/anie.201411190.

results are not easily understood in the framework of the simple oblate versus prolate theory proposed for engendering mononuclear lanthanide SMMs,[3] a point that was recently raised about the properties of another Er^{III} compound.[14]

The ligand $LiN(SiMe_3)_2$ was synthesized by reaction of excess *n*BuLi with $HN(SiMe_3)_2$ followed by recrystallization from a THF/hexanes mixture to yield the dimeric species $[\{Li(THF)\mu\text{-}N(SiMe_3)\}_2]$,[15] as confirmed by X-ray crystallography. The ligand was reacted with a stoichiometric amount of $ErCl_3$ in THF, the solution was reduced to a paste and then finally extracted with pentane, which led to the formation of light pink crystals of **1** (Figure 1) upon concentration and cooling down to −15 °C.

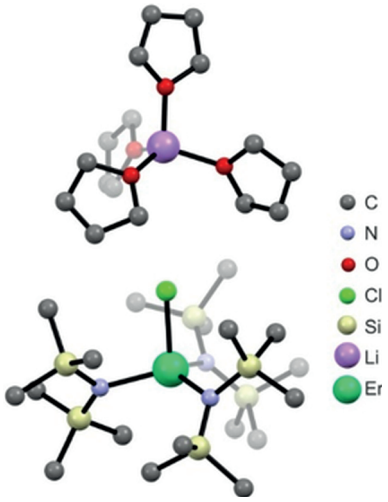

Figure 1. Crystal structure of $[Li(THF)_4][Er\{N(SiMe_3)_2\}_3Cl]\cdot 2THF$ (**1**) showing the molecular trigonal pyramidal geometry of the Er center and the $[Li(THF)_4]^+$ cation. Hydrogen atoms and solvent THF molecules omitted for clarity.

Compound **1** crystallizes in the monoclinic space group $P2_1/n$ (Supporting Information, Table S1). Selected bond distances and angles are provided in the Supporting Information, Tables S2, S3. The Er1−N bond distances are in the 2.231–2.251 Å range, which is slightly longer than reported for $[Er\{N(SiMe_3)_2\}_3]$,[11] and the Er1−Cl bond distance is 2.528(2) Å. The N-Er1-N angles are highly flattened with an average N-Er-N angle of 116.0°, which is closer to ideal trigonal-planar angles than $[Er\{N(SiMe_3)_2\}_3]$ (113.4°); the average value of the Cl-Er-N angles is 101.7°. The closest Er−Er distance is 11.175(2) Å, which justifies the assumption that the magnetic intermolecular dipole–dipole interactions are very weak.

The static magnetic properties of **1** were measured on a sample of crushed crystals using a MPMS SQUID magnetometer under a 1000 Oe dc field. The temperature dependence of the dc magnetic susceptibility of **1** is very similar to other Er compounds (see references in Table 1). The room-temperature χT value of 11.47 emu mol^{-1} K (Supporting Information, Figure S1) is consistent with an isolated Er^{III} center ($J = 15/2$, $g = 1.2$ with the expected χT value of 11.48 emu mol^{-1} K). At lower temperatures, the χT value slowly decreases to reach 9.55 emu mol^{-1} K at 2 K, which is attributed to the depopulation of m_J sublevels and magnetic anisotropy. The dynamic properties of **1** were investigated using ac magnetic susceptibility measurements in the frequency range 1–1500 Hz. The out-of-phase ac magnetic susceptibility versus frequency plot (Figure 2) recorded in the 1.8–11 K range under a zero applied dc magnetic field reveals slow magnetic relaxation behavior typical of SMMs (see the Supporting Information, Figure S2 for in-phase and out-of-phase ac susceptibility as a function of temperature). The relaxation times obtained from fitting the ac magnetic susceptibility data using the generalized Debye model[16] were plotted vs. $1/T$ to give an Arrhenius plot with two obvious regimes: a temperature-dependent regime above approximately 5 K and a temperature-independent regime below 5 K. The selected high-temperature linear region (7.5–11 K) of the Arrhenius plot was used to calculate the thermal energy barrier to the magnetization reversal $\Delta E_{eff}/k_B = 63.3$ K and $\tau_0 = 1.07 \times 10^{-7}$ s. The low-temperature regime is expected to be controlled by quantum tunneling effects (direct relaxation process). The Cole–Cole plot (Supporting Information, Figure S3) suggests the existence of only one thermal relaxation process, as evidenced by the semicircle overlay of χ'' and χ'

Table 1: Comparison of mononuclear erbium(III) single-molecule magnets.

Compound	U_{eff}/k_B [K]	Hysteresis [K]	dc field?	Source
1	66.4	3	No	[a]
1′	55.1	3	No	[a]
$[Er\{N(SiMe_3)_2\}_3]$	122	1.9[b]	No	[12]
$[Er(NHPhiPr_2)_3(THF)_2]$	25	–	Yes	[12]
[(Cp*)Er(COT)]	197, 323	5	No	[6a]
$[Er(COT)_2]$	216–286	10–12	No	[6b, 7]
[Er(trensal)]	77.7[c]	–	Yes	[14]
$[Er(COT'')_2]$	187	8	No	[6c]
$[Er_2(COT'')_3]$	335	14	No	[8]

[a] The current work. [b] Higher-temperature magnetic hysteresis measurement not attempted/reported. [c] Calculated.

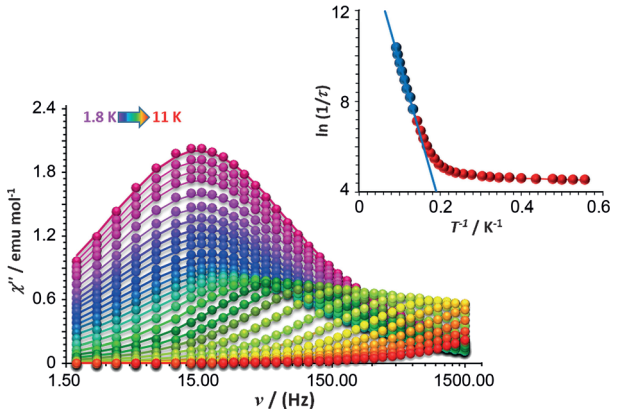

Figure 2. Imaginary component of the ac magnetic susceptibility data plotted versus frequency for **1**. Lines represent fitting of the experimental data at different temperatures using the generalized Debye model. Inset: Arrhenius plot of $\ln(1/\tau)$ vs T^{-1}. Fitting of the thermal regime is represented by linear fit of selected blue data points.

and α values below 0.29. On the other hand, because the Arrhenius plot does exhibit some curvature below 6.3 K, perhaps another relaxation pathway is also operative. Data in the entire 1.8–11 K temperature range were analyzed by the following equation:[17]

$$\tau_0^{-1} = AT + C + BT^n + \tau_0^{-1}\exp(-\Delta E_{eff}/k_B T) \quad (1)$$

where $AT+C$, BT^n, and $\tau_0^{-1}\exp(-\Delta E_{eff}/k_B T)$ represent direct, Raman, and Orbach relaxation processes, respectively. To fit the Arrhenius plot to Equation (1), the values of τ_0 and $\Delta E_{eff}/k_B$ were fixed based on the linear fit to the thermal regime (7.0–9.5 K; red dotted line, Figure 3). The values of the A and C parameters were also fixed based on the linear fit to the τ^{-1} vs T^1 dependence (direct process; gray dotted curve,

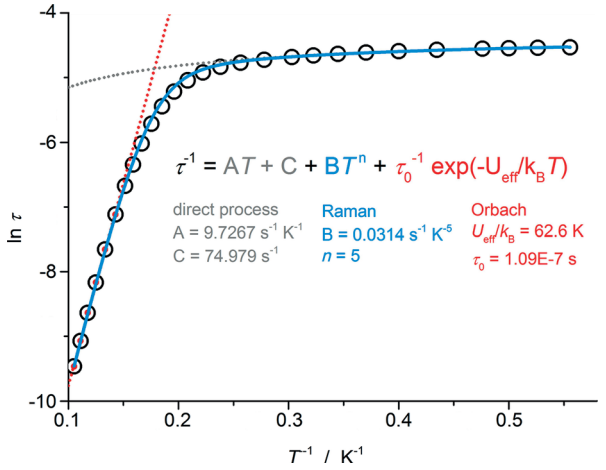

Figure 3. Fitting of Arrhenius plot based on Equation (1) and relaxation times obtained by simultaneous fitting of χ' and χ'' versus ν plots (Figure 2; Supporting Information, Figure S3). The red dotted line represents fitting of the Orbach/thermal regime; the gray dotted line represents fitting of the low-temperature regime. The variables obtained from these two fits were then fixed in the fitting of the full temperature regime (blue line), the curved part of which represents the Raman relaxation regime.

Figure 3) in the range of 1.8–3.1 K. With these restraints, the temperature range 1.8–9.5 K was fitted using Equation (1) assuming $n=5$, 7, or 9 and letting the B parameter to vary freely. The best fit was obtained for $n=5$ and $B=0.00585\ s^{-1}K^{-5}$ (Figure 3). Thus we conclude that the curvature of the Arrhenius plot is due to Raman relaxation.

Quantum tunneling is enhanced by weak intermolecular dipole–dipole interactions that can be suppressed by dilution in a diamagnetic matrix or by applying external dc field. A 10% diluted sample was prepared by combining an approximate 1:10 mass ratio of $[Li(THF)_4][Er\{N(SiMe_3)_2\}_3Cl]\cdot 2\,THF$ with the corresponding yttrium analogue in a THF/*n*-pentane mixture. Placing the solution in the freezer at −15 °C led to crystals of $[Er_{0.1}Y_{0.9}\{(Me_3Si)_2N\}_3(\mu\text{-}Cl)\{Li(THF)_3\}]\cdot$pentane (**1′**). Single-crystal XRD structural analysis revealed a slightly different crystal structure than what was observed for **1** in that the $[Li(THF)_3]^+$ cation is connected to the Cl^- bridge (Figure 4).[18] This difference leads to a slight change in the

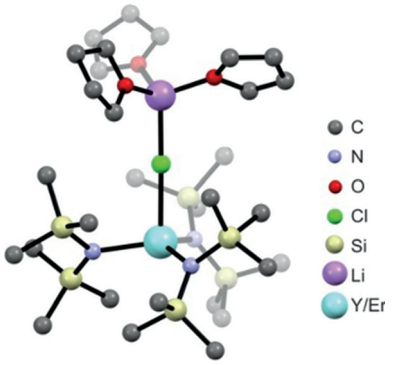

Figure 4. Molecular structure of $[Er_{0.1}Y_{0.9}\{(Me_3Si)_2N\}_3(\mu\text{-}Cl)\{Li(THF)_3\}]\cdot$pentane (**1′**). Hydrogen atoms and pentane molecules were omitted for the sake of clarity.

Cl-Er-N angles up to 8°, as well as a 0.14 Å difference in the Er–Cl bond distance compared to **1**. Ac measurements were performed on crushed crystals of the diluted sample, **1′**, revealing the retention of the out-of-phase signal with partial suppression of the quantum tunneling regime (Figure 5; Supporting Information, Figure S4). These results support the molecular nature of the slow magnetic relaxation in **1**. The ac data (Figure 5) were fitted using a generalized Debye model.[16] The resulting relaxation times were plotted vs. $1/T$ and the data reveal that there is a temperature-dependent regime above 3.8 K and a temperature-independent regime below 3.8 K. The high-temperature region (above 3.8 K) was fitted using the Arrhenius law, which resulted in an estimated effective energy barrier to the magnetization reversal of $\Delta E_{eff}/k_B = 55.8$ K and pre-exponential factor $\tau_0 = 2.84\times10^{-7}$ s. The estimated effective energy barriers for **1** and **1′** are different by about 7–8 K. We attribute this difference to the slightly altered coordination sphere of the two analogues, as well as the selection of points used to ascertain the energy barrier. The low-temperature regime for **1′** is most likely controlled by

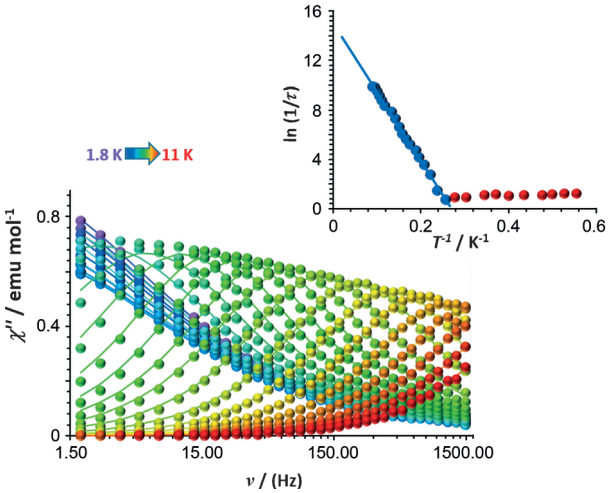

Figure 5. Imaginary component of the ac susceptibility plotted versus frequency for **1′**. Lines represent fitting of the experimental data at different temperatures using the generalized Debye model. Inset: Arrhenius plot of $\ln(1/\tau)$ vs T^{-1}. The blue line is the best fit of the thermal regime (blue data points).

quantum tunneling of the magnetization. When the ac measurements of **1′** are performed under a 1000 Oe static dc field, a further suppression of the quantum tunneling is observed as expected (Supporting Information, Figure S5). The ac data indicate very slow magnetic relaxation at temperatures below 3.1 K, on the order of 100 s; therefore, hysteresis measurements were performed at a conventional sweep rate of 34.6 Oe s^{-1}. The shape of the hysteresis loop at 1.8 K (Figure 6) for **1** is best described as waist-restricted or

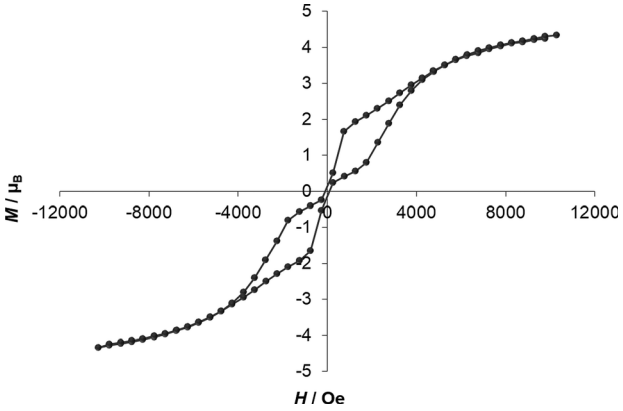

Figure 6. Magnetic hysteresis loop for **1** collected at 1.8 K and with 34.6 Oe s^{-1} sweep rate.

butterfly-like, similar to what was observed for other Er^{III} SMMs.[6b,8] A tunneling feature (reflection point) is observed at both negative and positive fields. The yttrium dilution sample exhibits sharper hysteresis out to 3 K (Supporting Information, Figure S6).

The magnetic parameters for compound **1** compared with other known mononuclear erbium(III) SMMs are compiled in Table 1. It is interesting at this stage to point out that the magnetic properties of the trigonal bipyramidal molecule $[Er(NHPh\mathit{i}Pr_2)_3(THF)_2]$ were compared to those of $[Er\{N(SiMe_3)_2\}_3]$ by Tang et al., and it was found that the former compound exhibits fast quantum tunneling, which is presumably due to increased transverse anisotropy owing to the presence of the two axial THF molecules.[12] The compound exhibits out-of-phase signals in the χ'' versus ν plots, albeit with the necessity of applying a dc field. Given these findings, we reasoned that the presence of the axial chloride ligand in **1** and **1′** might destroy the dynamic susceptibility properties but the effect of the chloride appears to only moderately destabilize the ground state, leading to a smaller effective energy barrier as compared to $[Er\{N(SiMe_3)_2\}_3]$.

Compound **1** is the first mononuclear erbium SMM with a negatively charged axial ligand that exhibits out-of-phase signals in the ac susceptibility data in the absence of an applied static dc field. Since other erbium(III) SMMs containing an axial ligand require the application of an external field to observe slow relaxation, the observed behavior of **1** was not anticipated. Nevertheless, the lower barrier observed for this new compound as compared to the trigonal $[Er\{N(SiMe_3)_2\}_3]$ complex is entirely reasonable.[3] The current findings support the hypothesis that erbium(III) ions in lower symmetry ligand environments other than those that are strictly limited to the oblate crystal-field geometry are prospects for interesting SMM behavior.

In summary, the first trigonal pyramidal erbium SMM is reported, the magnetic data of which indicate that strictly prolate f-electron density is not required to stabilize a crystal field that favors SMM behavior. The relaxation dynamics are interesting in that the presence of the axial chloride ligand does not lead to rapid relaxation of the magnetization at zero dc field. While the ligand framework may primarily stabilize the $m_J = 15/2$ ground state, it is noteworthy that this molecule exhibits strikingly different magnetic behavior than the trigonal bipyramidal compound $[Er(NHPh\mathit{i}Pr_2)_3(THF)_2]$. This work provides a good backdrop for future theoretical studies as it hints that simple models are not entirely adequate for accurate prediction of slow magnetic relaxation in lanthanide-based SMMs, a conclusion that is also supported by the study of Dy-based SMMs.[19] Additional experimental and theoretical studies are underway to explain the origins of zero-field SMM behavior for **1**. Importantly, the axial chloride poises this molecule to be a convenient precursor for the preparation of a family of derivatives and even the possibility of device applications by attaching the molecule to surfaces.

Experimental Section

Single-crystal X-ray data were collected at 110 K on a Bruker APEX II diffractometer equipped with a CCD detector. The data sets were recorded as ω-scans at 0.3° step width. Integration was performed with the Bruker SAINT software package and absorption corrections were empirically applied using SADABS. The crystal structures were refined using the SHELXL[20] suite of programs and the graphical interface Olex2.[21] Images of the crystal structure were rendered using the crystal structure visualization software DIAMOND or CCDC Mercury.[22] All of the structures were solved by direct methods. Any remaining non-hydrogen atoms were located by alternating cycles of least squares refinements and difference Fourier maps. All hydrogen atoms were placed at calculated positions (riding model). Anisotropic thermal parameters were added for all non-hydrogen atoms. A summary of pertinent information relating to unit cell parameters, data collection, and refinement statistics is provided in the Supporting Information. CCDC 1051281 (**1**) and CCDC 1051282 (**1′**) contain the supplementary crystallographic data for this paper. These data can be obtained free of charge from The Cambridge Crystallographic Data Centre via www.ccdc.cam.ac.uk/data_request/cif.

Magnetic susceptibility and magnetization measurements were collected using a Quantum Design MPMS-XL SQUID magnetometer. To prevent torqueing, the samples for magnetic measurements were prepared using crushed crystals immobilized in eicosane matrix sealed in quartz tubes. The dc magnetic susceptibility measurements were performed at an applied field of 1000 Oe over the temperature range 2–300 K. The ac magnetic susceptibility measurements were performed in a 5 Oe oscillating field at operating frequencies of 1–1500 Hz. The data were corrected for diamagnetic contributions of the sample holder and as calculated from the Pascal constants. Further synthetic details are given in the Supporting Information.

Keywords: erbium · magnetic hysteresis · mononuclear · prolate lanthanides · single-molecule magnets

How to cite: *Angew. Chem. Int. Ed.* **2015**, *54*, 5864–5868
Angew. Chem. **2015**, *127*, 5962–5966

[1] D. N. Woodruff, R. E. P. Winpenny, R. A. Layfield, *Chem. Rev.* **2013**, *113*, 5110 – 5148.
[2] a) P. C. E. Stamp, A. Gaita-Arino, *J. Mater. Chem.* **2009**, *19*, 1718 – 1730; b) W. Wernsdorfer, *Int. J. Nanotechnol.* **2010**, *7*, 497 – 522; c) G. Aromí, D. Aguila, P. Gamez, F. Luis, O. Roubeau, *Chem. Soc. Rev.* **2012**, *41*, 537 – 546; d) M. Jenkins, T. Hummer, M. J. Martinez-Perez, J. Garcia-Ripoll, D. Zueco, F. Luis, *New J. Phys.* **2013**, *15*, 095007.
[3] J. D. Rinehart, J. R. Long, *Chem. Sci.* **2011**, *2*, 2078 – 2085.
[4] J. D. Rinehart, M. Fang, W. J. Evans, J. R. Long, *J. Am. Chem. Soc.* **2011**, *133*, 14236 – 14239.
[5] P. Zhang, Y. N. Guo, J. K. Tang, *Coord. Chem. Rev.* **2013**, *257*, 1728 – 1763.
[6] a) S. D. Jiang, B. W. Wang, H. L. Sun, Z.-M. Wang, S. Gao, *J. Am. Chem. Soc.* **2011**, *133*, 4730 – 4733; b) K. R. Meihaus, J. R. Long, *J. Am. Chem. Soc.* **2013**, *135*, 17952 – 17957; c) J. J. Le Roy, I. Korobkov, M. Murugesu, *Chem. Commun.* **2014**, *50*, 1602 – 1604; d) K. S. Pedersen, L. Ungur, M. Sigrist, A. Sundt, M. Schau-Magnussen, V. Vieru, H. Mutka, S. Rols, H. Weihe, O. Waldmann, L. Chibotaru, J. Bendix, J. Dreiser, *Chem. Sci.* **2014**, *5*, 1650 – 1660.
[7] L. Ungur, J. J. Le Roy, I. Korobkov, M. Murugesu, L. F. Chibotaru, *Angew. Chem. Int. Ed.* **2014**, *53*, 4413 – 4417; *Angew. Chem.* **2014**, *126*, 4502 – 4506.
[8] J. J. Le Roy, L. Ungur, I. Korobkov, L. F. Chibotaru, M. Murugesu, *J. Am. Chem. Soc.* **2014**, *136*, 8003 – 8010.
[9] a) M. H. Xie, X. Y. Liu, S. W. Wang, L. Liu, Y. Y. Wu, G. S. Yang, S. L. Zhou, E. H. Sheng, Z. X. Huang, *Chin. J. Chem.* **2004**, *22*, 678 – 682; b) E. Sheng, S. Wang, G. Yang, S. Zhou, L. Cheng, K. Zhang, Z. Huang, *Organometallics* **2003**, *22*, 684 – 692; c) S. A. Schuetz, V. W. Day, R. D. Sommer, A. L. Rheingold, J. A. Belot, *Inorg. Chem.* **2001**, *40*, 5292 – 5295; d) M. Westerhausen, M. Hartmann, A. Pfitzner, W. Schwarz, *Z. Anorg. Allg. Chem.* **1995**, *621*, 837 – 850; e) F. T. Edelmann, A. Steiner, D. Stalke, J. W. Gilje, S. Jagner, M. Hakansson, *Polyhedron* **1994**, *13*, 539 – 546; f) R. A. Andersen, D. H. Templeton, A. Zalkin, *Inorg. Chem.* **1978**, *17*, 2317 – 2319; g) D. C. Bradley, J. S. Ghotra, F. A. Hart, *J. Chem. Soc. Dalton Trans.* **1973**, 1021 – 1023; h) E. C. Alyea, D. C. Bradley, R. G. Copperthwaite, *J. Chem. Soc. Dalton Trans.* **1972**, 1580 – 1584.
[10] a) A. M. Bryan, G. J. Long, F. Grandjean, P. P. Power, *Inorg. Chem.* **2013**, *52*, 12152 – 12160; b) A. Eichhöfer, Y. Lan, V. Mereacre, T. Bodenstein, F. Weigend, *Inorg. Chem.* **2014**, *53*, 1962 – 1974.
[11] E. D. Brady, D. L. Clark, J. C. Gordon, P. J. Hay, D. W. Keogh, R. Poli, B. L. Scott, J. G. Watkin, *Inorg. Chem.* **2003**, *42*, 6682 – 6690.
[12] P. Zhang, L. Zhang, C. Wang, S. Xue, S.-Y. Lin, J. Tang, *J. Am. Chem. Soc.* **2014**, *136*, 4484 – 4487.
[13] a) S. L. Zhou, S. W. Wang, G. S. Yang, X. Y. Liu, E. H. Sheng, K. H. Zhang, L. Cheng, Z. X. Huang, *Polyhedron* **2003**, *22*, 1019 – 1024; b) Q. Wu, J. Zhou, Z. Yao, F. Xu, Q. Shen, *J. Org. Chem.* **2010**, *75*, 7498 – 7501.
[14] E. Lucaccini, L. Sorace, M. Perfetti, J. P. Costes, R. Sessoli, *Chem. Commun.* **2014**, *50*, 1648 – 1651.
[15] a) H. Mack, G. Frenzen, M. Bendikov, M. S. Eisen, *J. Organomet. Chem.* **1997**, *549*, 39 – 43; b) L. M. Engelhardt, B. S. Jolly, P. C. Junk, C. L. Raston, B. W. Skelton, A. H. White, *Aust. J. Chem.* **1986**, *39*, 1337 – 1345.
[16] D. Gatteschi, R. Sessoli, R. Villain, *Molecular Nanomagnets*, Oxford University Press, New York, **2006**.
[17] K. R. Meihaus, S. G. Minasian, W. W. Lukens, S. A. Kozimor, D. K. Shuh, T. Tyliszczak, J. R. Long, *J. Am. Chem. Soc.* **2014**, *136*, 6056 – 6068.
[18] Compound **1** also crystallizes in the $P2_1/c$ space group with exactly the same coordination sphere as found for compound **1′**, but the X-ray data were poor. For details and discussion, see the Supporting Information, Figures S7–S9.
[19] D. Aravena, E. Ruiz, *Inorg. Chem.* **2013**, *52*, 13770 – 13778.
[20] G. Sheldrick, *Acta Crystallogr. Sect. A* **2008**, *64*, 112 – 122.
[21] O. V. Dolomanov, L. J. Bourhis, R. J. Gildea, J. A. K. Howard, H. Puschmann, *J. Appl. Crystallogr.* **2009**, *42*, 339 – 341.
[22] a) L. J. Barbour, *J. Supramol. Chem.* **2001**, *1*, 189 – 191; b) C. F. Macrae, P. R. Edgington, P. McCabe, E. Pidcock, G. P. Shields, R. Taylor, M. Towler, J. van de Streek, *J. Appl. Crystallogr.* **2006**, *39*, 453 – 457.

Received: November 18, 2014
Revised: January 14, 2015
Published online: March 24, 2015

